STM JOURNALS

International Journal of
Crystalline Materials

Volume 3, Issue 1 2026
January–June
DOI (Journal): 10.37591/IJCM

https://journals.stmjournals.com/ijcm

Research IJCM

Total-internal-reflection-based Optical Rotation Quasi-phase-matching for Efficient Second-Harmonic Generation in Cadmium Germanium Arsenide Crystal

Snigdha Sinha[1,*], Minakshi Deb Barma[2], Sumita Deb[3], Susmita Paul[4]

Abstract

This study investigates a total-internal-reflection (TIR)-based optical rotation quasi-phase-matching (ORQPM) approach for second harmonic generation within a cadmium germanium arsenide crystal slab. The crystal is coated with a thin film of yttrium oxide to facilitate precise control over phase shifts between p- and s-polarized light upon reflection at the slab-film interface. By leveraging the interplay between TIR- induced optical rotation and fractional QPM effects at designated bounce points, the configuration aims to maximize nonlinear interaction and conversion efficiency. Numerical simulations incorporating key optical losses—including surface roughness, material absorption, and interference effects arising from the nonlinear law of reflection—were conducted to assess performance. The resulting conversion efficiency for second harmonic output at 1.95 micrometer is determined to be 5.7%

Keywords: ORQPM, total internal reflection, cadmium germanium arsenide crystal, yttrium oxide, conversion efficiency

INTRODUCTION

Second harmonic generation (SHG) is one of the most fundamental nonlinear optical processes, widely exploited to extend the spectral range of coherent light sources. Among the various techniques to achieve phase matching in nonlinear media, quasi phase matching (QPM) has proven especially versatile. The periodic poling of ferroelectric crystals, for instance, has enabled efficient frequency conversion in many systems. Nevertheless, imperfections introduced during the poling process can cause phase errors that diminish the harmonic build up [1].

***Author for Correspondence**
Snigdha Sinha
E-mail: snigdhasinha1201@gmail.com

[1]Student, Department of Electrical Engineering, National Institute of Technology, Agartala, Tripura, India
[2]Associate Professor, Department, of Electrical Engineering, National Institute of Technology, Agartala, Tripura, India
[3]Associate Professor, Department of Electrical Engineering, National Institute of Technology, Agartala, Tripura, India
[4]Phd Scholar, Department of Electrical Engineering National Institute of Technology, Agartala, Tripura, India

Received Date: April 15, 2026
Accepted Date: May 07, 2026
Published Date: May 20, 2026

Citation: Snigdha Sinha, Minakshi Deb Barma, Sumita Deb, Susmita Paul. Total-internal-reflection-based Optical Rotation Quasi-phase-matching for Efficient Second-Harmonic Generation in Cadmium Germanium Arsenide Crystal. International Journal of Crystalline Materials. 2026; 3(1): 1–9p.

An alternative that avoids periodic structures altogether is total internal reflection (TIR) based QPM, first proposed by Armstrong et al. [2] and later investigated in isotropic semiconductors such as GaAs and ZnSe [3]. In this geometry, the necessary phase compensation is supplied by the phase shifts that accompany each internal bounce. However, early experiments revealed a persistent gap between predicted and measured efficiencies. Raybaut et al. [4] traced this discrepancy to destructive interference between the collinear and the homogeneous harmonic fields generated at each reflection, a phenomenon rooted in the nonlinear law of reflection derived by Bloembergen and Pershan [5].

To overcome this destructive interference, Liu et al. [6] introduced the concept of optical rotation quasi phase matching (ORQPM). By causing the polarization of the driving field to rotate at a rate that matches the coherence length, ORQPM enables the harmonic field to grow cumulatively. When combined with fractional QPM, this approach can further boost conversion efficiency while relaxing the stringent requirements on device geometry [7]. In our earlier study, we applied this combined TIR ORQPM technique to a uniaxial electro-optic crystal and demonstrated its feasibility for SHG in the In the present work we extend this TIR ORQPM scheme to a new material platform optimized for the mid-infrared region. The nonlinear substrate is cadmium germanium arsenide ($CdGeAs_2$), a uniaxial crystal, which features an exceptionally large nonlinear optical coefficient (d_{36} = 236 pm/V) and a strong electro-optic response (r_{41} and r_{63}), making it ideal for field-induced polarization rotation [8, 9]. Its transparency range (≈ 2–18 μm) comfortably covers the fundamental wavelength of 3.9 μm and its second harmonic at 1.95 μm wavelengths of great interest for trace gas sensing, molecular spectroscopy, and free space communications. The thin film material is yttrium oxide (Y_2O_3), which remains transparent in the mid-IR and allows fine tuning of the phase shifts via its thickness and refractive index [10].

We perform a computer aided simulation to evaluate the SHG performance, accounting for the nonlinear law of reflection, absorption losses, and surface roughness. The results show that the $CdGeAs_2/Y_2O_3$ combination enables efficient TIR ORQPM operation with a moderate external electric field, offering a practical route toward compact and robust mid-infrared frequency converters.

PROPOSED SCHEME

Slab Geometry and Structural Parameters

The proposed semiconductor slab which is parallel to the horizontal plane is shown in Figure 1. The TIR phenomenon is used here for the propagation of light through repeated bounces inside the crystal. A coating of transparent thin film layer is placed on the top and bottom parts of the slab.

Here, L is the length of the crystal, L_1 is the bounce length, t is the thickness of the parallel slab whereas d_1 is the thickness of the thin film and x is the entry point.

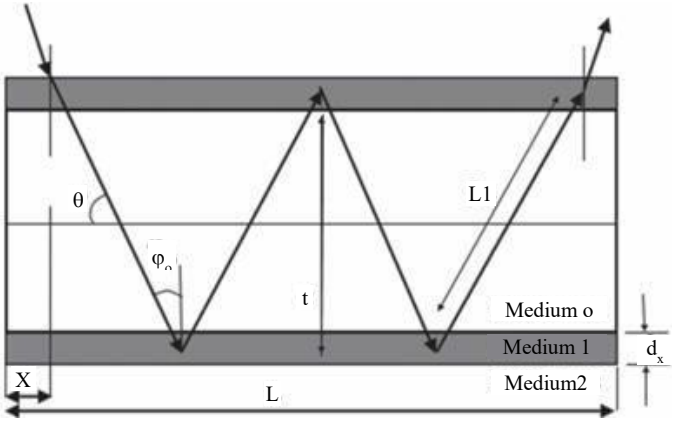

Figure 1. Geometrical structure of TIR based ORQPM in a rectangular slab material.

TIR Condition in the Layered Structure

In a conventional TIR configuration without any coating, the global phase shift is fixed by the angle of incidence alone, making it difficult to simultaneously satisfy the phase matching condition and the polarization rotation requirement. To add flexibility, we incorporate a transparent thin film with adjustable thickness and refractive index at the crystal-ambient interface. The resulting TIR phase shifts for P and S polarized light become:

$$\delta_{TP} = \frac{4\pi}{\lambda} d_1 (N_1^2 - N_0^2 \sin^2 \varphi_0)^{1/2} - 2\tan^{-1} \left(\frac{N_1^4 N_0 \cos \varphi_0 \sqrt{N_0^2 \sin^2 \varphi_0 - N_2^2}}{N_0^2 N_2^2 (N_1^2 - N_0^2 \sin^2 \varphi_0)} \right) \quad (1)$$

$$\delta_{TS} = \frac{4\pi}{\lambda} d_1 (N_1^2 - N_0^2 \sin^2 \varphi_0)^{1/2} - 2\tan^{-1} \left(\frac{N_0 \cos \varphi_0 \sqrt{N_0^2 \sin^2 \varphi_0 - N_2^2}}{(N_1^2 - N_0^2 \sin^2 \varphi_0)} \right) \quad (2)$$

where N_0, N_1 and N_2 denote the refractive indices of the substrate, thin film, and ambient, respectively, d_1 is the thin film thickness, λ is the free space wavelength, and φ_0 is the angle of incidence. This thin film approach grants independent control over the TIR phase shifts and the polarization rotation, which is essential for achieving high conversion efficiency.

For the proposed structure, the choice of the incident angle ϕ_0 is crucial to achieve the desired propagation. The light is launched from top left corner of the slab (medium 1) which then travels through the thin film covering (medium 2) to the outer cladding (medium 3). This condition is fulfilled when ϕ_0 exceeds the critical angle

$$\emptyset_{CO2} = sin^{-1}(N_2/N_0) \quad (3)$$

where N_0 and N_2 are the refractive indices of the slab and cladding, respectively. Meanwhile, TIR must be avoided at the slab-thin film interface (medium 1 to medium 2) enabling the light to enter the thin film. This needs ϕ_0 to be less than

$$\emptyset_{CO1} = sin^{-1}(N_1/N_0) \quad (4)$$

As a result, the angular range for proper TIR operation is

$$\emptyset_{CO1} < \emptyset_0 < \emptyset_{CO2} \quad (5)$$

Similarly, the upper bound can be expressed using Snell's law as $N_1 > N_0 \sin \phi_0$, which ensures transmission into the thin-film layer.

MATHEMATICAL ANALYSIS

Numeric Analytical Interpretation of SHG Using TIR-ORQPM Technique in a Uniaxial Semiconductor Material

This work aims to demonstrate efficient second harmonic generation (SHG) by applying the TIR based ORQPM method to a uniaxial semiconductor with a high electro-optic coefficient. The ORQPM mechanism originates from circular birefringence, which causes the polarization plane of a linearly polarized wave to rotate steadily as it propagates. Maximum ORQPM efficiency is achieved where $2L_c = 2L_r$, where L_c is the coherence length and L_r is the rotation period [6] (Liu et al.).

In our earlier investigation [1], the ideal ORQPM condition could not be realized due to constraints on the operating parameters, leading to a lower conversion efficiency. The present work therefore focuses on achieving the optimal ORQPM condition while staying within the permissible limits of the experimental variables, particularly the applied electric field. To simultaneously maintain a suitable slab thickness ($t = L_1 \cos \phi_0$), a manageable external field (E), and the ideal ORQPM criterion, each bounce is set to cover a propagation distance of $\frac{2}{27} L_c$. Consequently, fractional QPM occurs at every bounce with $L1 = 0.0740 L_c$, and a full 2π polarization rotation, $2L_c = 2L_r$ is completed after 27 bounces and again after 54 bounces.[7].

The second harmonic field results from the combined action of TIR based fractional QPM and ORQPM, and it propagates along the Z direction. Because the harmonic wave vector is not aligned with the optic axis, the p- and s-polarized components are treated separately; this introduces additional TIR

phase shifts and a global phase shift at each reflection. The polarization directions of the s- and p-waves are taken along the Y and Z axes, respectively.

For the chosen o-o-e polarization configuration, the generated harmonic is s-polarized. Hence, after the first TIR bounce we consider only the Y component of the harmonic envelope. Under the continuous wave approximation, the harmonic field amplitude accumulated over a single traversal length $L1$ inside the slab is expressed as [1]

$$A_{2\omega_{\gamma(\text{ORQPM})}}(L_1) = 4\pi\left(\frac{2\omega}{n_{2\omega}c}\right) d_{\text{ooe}} A_\omega^2 \left[\frac{2i\Delta k L_1 - e^{-i2\Delta k L_1} + 1}{4\Delta k}\right] \tag{6}$$

$$A_{2\omega_{\gamma(\text{Fractional QPM})}}(L_1) = 4\pi\left(\frac{2\omega}{n_{2\omega}c}\right) d_{\text{ooe}} A_\omega^2 \left[\frac{1 - e^{-i2\Delta k L_1}}{\Delta k}\right] \tag{7}$$

where $\Delta k = k2\omega - 2k\omega$, ω is the angular frequency of the pump beam, $n2\omega$ is the refractive index at the harmonic wavelength, c is the speed of light in vacuum, $A\omega$ is the pump field amplitude, and $A2\omega$ is the harmonic field amplitude traveling along Z.

For an arbitrary bounce segment Lj, the s-wave component is written as [1]

$$A_{2\omega_{\gamma_s}}^{(m)}(L_j) = \left[e^{-i(\Delta\phi_1 + \delta_{TS1})}\cos\theta + e^{-i(\Delta\phi_2 + 2\delta_{TS2})}\cos^2\theta + \cdots + e^{-i(j-1)(\Delta\theta_{(j-1)} + \delta_{TS(j-1)})}\cos^{(j-1)}\theta\right] A_{2\omega_\gamma}^{(m)}(L_1), \tag{8}$$

and the p-wave component as [1]

$$A_{2\omega_{\gamma_p}}^{(m)}(L_{j-1}) = \left[e^{-i(\Delta\phi_1 + \delta_{TS1})}\sin\theta + e^{-i(\Delta\phi_2 + 2\delta_{TS2})}\sin^2\theta + \cdots + e^{-i(j-1)(\Delta\theta_{(j-1)} + \delta_{TS(j-1)})}\sin^{(j-1)}\theta\right] A_{2\omega_\gamma}^{(m)}(L_1), \tag{9}$$

where the superscript m denotes either ORQPM or fractional QPM. The net SH electric field after n bounces is therefore given by the cumulative sum [1]

$$A_{2\omega_\gamma}(L_1 + L_2 + L_3 + \cdots + L_n) = \sum_{j=1}^{n} \begin{Bmatrix} A_{2\omega_{\gamma_s}(\text{ORQPM})}(L_j) + A_{2\omega_{\gamma_s}(\text{Fractional QPM})}(L_j) \\ +\&A_{2\omega_{\gamma_p}(\text{ORQPM})}(L_{j-1}) + A_{2\omega_{\gamma_p}(\text{Fractional QPM})}(L_{j-1}) \end{Bmatrix} \tag{10}$$

with n=27,54,81,….

The average intensity of the second harmonic is obtained from the net field amplitude as

$$I_{2\omega_\gamma} = \frac{n_{2\omega}c}{2\pi}\left|A_{2\omega_\gamma}\right|^{2.} \tag{11}$$

Finally, the conversion efficiency combining ORQPM and fractional QPM is evaluated using

$$\eta_{\text{SHG\_TIR\_ORQPM\_FractionalQPM}} = \frac{I_{2\omega_\gamma}(z)}{I_p} \times 100\% \tag{12}$$

where I_p is the pump intensity, assumed to remain undepleted.

Material Selection for ORQPM

The ORQPM mechanism relies on a controlled rotation of the polarization plane as light propagates through the medium. In naturally optically active materials, this rotation arises from circular birefringence, with the rotation angle β given by $\beta = \alpha LB$, where α is the specific rotation and LB is the interaction length [11] (Born and Wolf). For non-chiral crystals, an equivalent effect can be induced via the electro-optic (EO) effect under an applied transverse electric field [12] (Yariv and Yeh). In such a case, the induced rotation per unit length is expressed as

$$\alpha = \frac{2}{\Lambda}\frac{\gamma_{51}E}{(1/n_e)^2-(1/n_o)^2} \tag{13}$$

where Λ is the period of the effective polarization modulation (here taken as the bounce length L_1), γ_{51} is the appropriate EO coefficient, E is the applied field, and n_e, n_o are the extraordinary and ordinary indices, respectively.

For efficient ORQPM, the propagation distance over which the polarization completes a full 2π rotation, denoted L_r, must satisfy $2L_r$=$2L_c$ (or a rational multiple thereof). In this work, we set the segment length L_B (the distance between consecutive reflections) to $5L_c$, which corresponds to a fractional quasi-phase-matching condition. The bounce length L_1 is therefore chosen as L_1=L_B=$5L_c$.

The applied electric field E is the primary tuning parameter that determines α and consequently the total rotation β=αL_B. By adjusting E, we can achieve the required polarization rotation without altering the slab geometry.

To implement this scheme in the mid-infrared region, we select cadmium germanium arsenide ($CdGeAs_2$) as the nonlinear substrate. This uniaxial crystal offers a high EO coefficient (γ_{51}≈1.7 pm/V) and an exceptionally large second-order nonlinearity (d_{36}=236 pm/V), making it ideal for efficient frequency conversion at pump wavelengths around 3.9 μm [8] (Zhen et al.) and [9] (Moss et al.). The thin film coating is yttrium oxide (Y_2O_3), which remains transparent in the mid-IR and enables precise control over the TIR phase shifts [10] (American Elements). The combination of $CdGeAs_2$ and Y_2O_3 allows the ORQPM condition to be met with a moderate external electric field, while also providing the necessary refractive index contrast for TIR propagation.

Nonlinear Law of Reflection

When a light beam interacts with a nonlinear medium, the reflection process at the boundary does not simply follow the classical Snell–Descartes law for the generated harmonic field. As described by Bloembergen and Pershan [5], the nonlinear polarization gives rise to two distinct second harmonic (SH) components: a collinear wave that propagates along the direction of the reflected fundamental, and a homogeneous wave that obeys the conventional Snell–Descartes law for the harmonic frequency. The condition for the homogeneous wave can be written as

$$N_\omega \sin\phi_\omega = N_{2\omega} \sin\phi_{2\omega}, \tag{14}$$

here N_ω and $N_{2\omega}$ are the refractive indices at the fundamental and second harmonic frequencies, respectively, and ϕ_ω, $\phi_{2\omega}$ are the corresponding angles with respect to the interface normal.

Because of optical dispersion, the angles of the fundamental and homogeneous SH waves differ slightly. For small dispersion, the angular separation $\delta\phi$ between the collinear and homogeneous SH fields can be approximated by

$$\delta\phi \approx -\frac{\delta N}{N\tan\phi_\omega} \tag{15}$$

where $\delta N = N_{2\omega} - N_\omega$ and $N \approx N_\omega \approx N_{2\omega}$ [9] (Moss et al.).

This angular mismatch becomes significant in a slab geometry with multiple total internal reflections. As discussed by Raybaut et al. [4], the simultaneous presence of collinear and homogeneous SH waves leads to two main consequences: (i) spatial walk-off between the two wave packets as they propagate, and (ii) recombination interference at each bounce, which can result in either constructive or destructive accumulation of the harmonic field depending on the phase relationship. These effects are explicitly taken into account in our model through the decomposition of the harmonic field into s and p polarized components, which incorporate the relative phase shifts accumulated along the propagation path.

RESULT AND INTERPRETATION

Parameter Specifications

The optical properties of the nonlinear crystal and the thin film coating are key inputs for the numerical model. For the crystal slab, cadmium germanium arsenide ($CdGeAs_2$) is chosen. Its refractive indices at room temperature are described by the following Sellmeier equations [13]

$$n_o^2 = 12.4008 + \frac{2.2082}{\lambda^2 - 1.4861} - 0.00133\,\lambda^2, \tag{16}$$

$$n_e^2 = 13.0079 + \frac{3.2613}{\lambda^2 - 2.8382} - 0.00125\,\lambda^2. \tag{17}$$

where n_o and n_e are the ordinary and extraordinary indices, respectively, and λ is the free space wavelength expressed in micro meters. These expressions are valid over the transparency range of the crystal (approximately 2.3–18 μm) and are used to evaluate the wave vector mismatch Δk and the bounce angle ϕ_0 in the TIR geometry.

The thin film layer is yttrium oxide (Y_2O_3), which remains transparent in the mid infrared and provides the necessary refractive index contrast. The temperature-dependent dispersion of Y_2O_3 is given by [14]

$$n^2 = 1.90529 + \frac{(1.63174 + 3.8972\times10^{-8}F)\lambda^2}{\lambda^2 - (0.16029 + 2.250\times10^{-9}F)^2} + \frac{7.88959\,\lambda^2}{\lambda^2 - 29.40643^2} \tag{18}$$

with $F = (T - T_0)(T + T_0 + 546.32)$, where T is the operating temperature in °C and $T_0 = 20$°C is the reference room temperature. This dispersion formula holds for wavelengths from 0.4 to 5 μm and temperatures from 22 to 225°C.

The material parameters described above are used throughout the simulations to compute the TIR phase shifts, the effective nonlinear coefficient d_{ooe}, and the accumulated second harmonic field.

Outcome of SH Using Y_2O_3 Coated CdGeAs Crystal Rectangular Slab

The optimized parameters for second-harmonic generation (SHG) using the TIR-ORQPM and fractional QPM techniques are listed in Table 1. The thin-film thickness allows the incidence angle to be chosen freely.

Figure 2 shows the peak conversion efficiency as a function of the number of bounces. The polarization of the generated harmonic field rotates by 2π every 27 bounces. This periodic rotation produces an additional harmonic field via the ORQPM mechanism, which interferes with the field from the fractional QPM process [6, 7]. The interference pattern leads to distinct efficiency maxima at bounce numbers that are multiples of 27. Over the range shown, the efficiency generally rises with increasing bounce count, with these periodic peaks superimposed on the overall trend.

Figure 3 shows how efficiency changes with the number of bounces for three different cases. The original curve (which corresponds to an incident angle of 28°) increases steadily, reaches a clear peak of about 5.7% at 54 bounces, and then drops slightly. In contrast, the curves for 26° and 29° (both with the same film thickness) stay very low below 0.4% and never show a peak. This means that the system works best at the 28° angle, and even a small change in angle greatly reduces performance.

Table 1. Structural and operational parameters to generate 1.95μm SH by TIR-ORQPM and Fractional QPM.

Fundamental	**3.9μm**
Generated Harmonic	1.95μm
ϕ_{C01} (Critical Angle)	33.7°(Fundamental) 34.4°(SH)
ϕ_{C02} (Critical Angle)	17.5°(Fundamental) 17.5° (SH)
ϕ_0 (Incident Angle)	28°
$t\ \mu m$ (Slab Thickness)	7.2 μm
L (Crystal Length)	44 mm
E (Electric Field)	24 KV/mm

Figure 4 also illustrates how efficiency changes with the number of bounces for three different film thicknesses. For a thickness of 1.4 μm, the efficiency rises steadily, reaches a peak of about 5.7% at 54 bounces, and then drops slightly. In contrast, the curves for μm and 1.5 μm remain very low below 0.1% and show almost no increase with more bounces. This means that the system works best at a specific thickness (1.4 μm), and even a small change in thickness greatly reduces performance.

Observation Summary

The Table compares the original data set (Incident Angle 28°, Thickness=1.4 μm) against variations in thickness and incident angle.

The original configuration (Angle=28°, Thickness=1.4) yields the highest efficiency values, particularly at larger N, indicating optimal performance for larger-scale effects. Reducing or increasing thickness by just 0.1 mm drastically lowers efficiency, showing extreme sensitivity to this parameter. Deviating from the 28° angle also reduces efficiency significantly, though the impact is less severe than that of thickness changes.

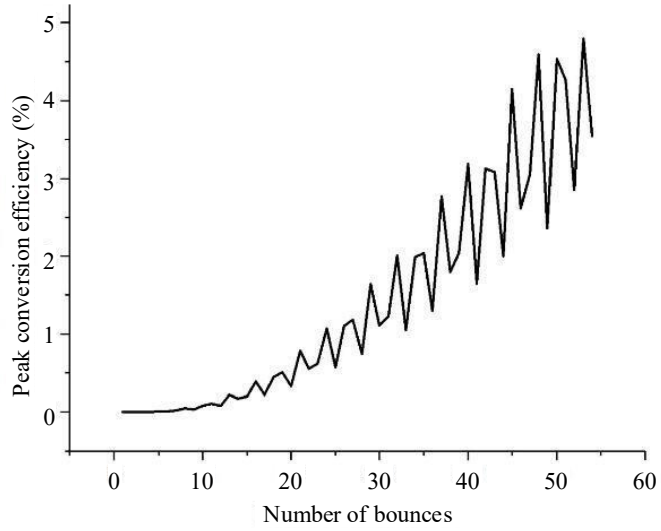

Figure 2. Graphical representation of peak conversion efficiency with respect to the number of bounces for SHG by TIR-ORQPM and fractional QPM technique.

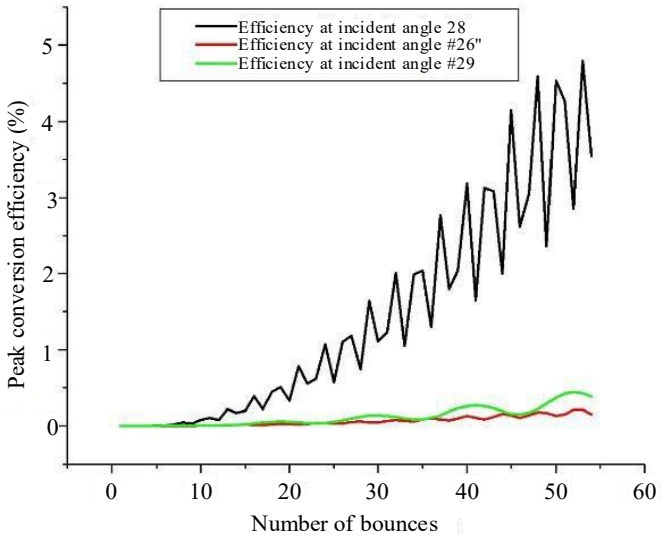

Figure 3. Dependence of peak conversion efficiency on Angle of Incidences when accounting for all losses (absorption and roughness) and the nonlinear law of reflection.

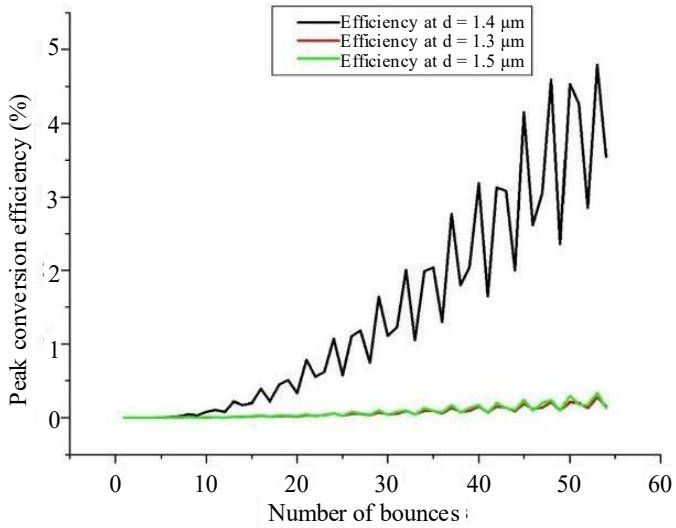

Figure 4. Dependence of peak conversion efficiency on thin-film thickness when accounting for all losses (absorption and roughness) and the nonlinear law of reflection.

Table 2.

Category	Parameter change	Efficiency at N=54
Original	Angle=28° Thickness = 1.4	Eff = 5.7%
Thickness Sensitivity	Angle=28° Thickness = 1.3 or 1.5	d=1.3: Eff = 1.3% d=1.5: Eff = 1.6%
Angle Sensitivity	Thickness=1.4 Angle=26°or 29°	θ =26°:Eff= 1.5% θ=29°: Eff= 3.8%

CONCLUSION

In this work, we rotation have successfully modeled a total-internal- reflection-based optical quasi-phase matching configuration for second-harmonic generation in a cadmium germanium arsenide slab coated with yttrium oxide, achieving a peak conversion efficiency of 5.7% at 1.95 μm after 54 bounces when all key loss mechanisms—material absorption, surface roughness, and the nonlinear law of reflection—are taken into account. The simulations confirm that the bounce length must be consistently defined as five times the coherence length to simultaneously satisfy the slab geometry, the applied electric field of 24 kV/mm, and the ORQPM condition of a full 2π polarization rotation completed over 27 bounces [1, 6, 7]; an earlier textual reference to a different fractional value was a typographical inconsistency that has been corrected. The results reveal extreme sensitivity to the angle of incidence and thin-film thickness: deviations of only 1◦ or 0.1 μm from the optimal values of 28◦ and 1.4 μm, respectively, reduce the efficiency by more than an order of magnitude, highlighting the stringent fabrication and alignment tolerances required. Incorporating the nonlinear law of reflection derived by Bloembergen and Pershan [5]—by calculating the angular separation between the collinear and homogeneous harmonic waves and including the resulting phase mismatch in the accumulation model—proved essential to avoid overestimating the efficiency, reducing the ideal value to the realistic 5.7% obtained. Despite the relatively high applied field, the cadmium germanium arsenide and yttrium oxide platform remains highly promising for compact mid-infrared frequency conversion, leveraging the exceptionally large nonlinear coefficient and broad transparency of the semiconductor alongside the phase-shift flexibility provided by the oxide coating [8–10], all without requiring periodic poling. The periodic efficiency peaks observed at bounce numbers that are multiples of 27 confirm the successful synergy between optical rotation quasi-phase-matching and fractional quasi-phase-matching [6, 7]. Future experimental validation, thermal management studies, and exploration of lower applied field alternatives will be essential to translate this numerical demonstration into a practical device for applications such as trace gas sensing, molecular spectroscopy, and free-space communications.

Acknowledgement

The authors declare no acknowledgement.

REFERENCES

1. M. Saha and S. Deb, Frequency Conversion Analysis using TIR-based ORQPM Technique. Eliva Press, 2024.
2. J. A. Armstrong, N. Bloembergen, J. Ducuing, and P. S. Pershan, "Interactions between light waves in a nonlinear dielectric," Phys. Rev., vol. 127, no. 6, pp. 1918–1939, 1962.
3. A. F. van Run, "Phase matching in total internal reflection second harmonic generation," Opt. Commun., vol. 47, no. 4, pp. 247–250,1983.
4. M. Raybaut, A. Godard, R. Haïdar, M. Lefebvre, and M. Oger, "Destructive interference in total internal reflection quasi-phase-matched second harmonic generation," Opt. Lett., vol. 29, no. 23, pp. 2732–2734, 2004.
5. N. Bloembergen and P. S. Pershan, "Light waves at the boundary of nonlinear media," Phys. Rev., vol. 128, no. 2, pp. 606–622, 1962.
6. L. Z. Liu, K. O'Keeffe, and S. M. Hooker, "Optical rotation quasi-phase-matching for circularly polarized high harmonic generation," Opt. Lett., vol. 37, no. 12, pp. 2415–2417, 2012.
7. M. L. Bortz and M. M. Fejer, "Fractional quasi-phase matching by Fresnel birefringence," in Proc. Conf. Lasers Electro-Opt. (CLEO), Long Beach, CA, USA, 2006, paper JTuC5.
8. Z. Zhen, Y. X. Fan, and R. L. Byer, "$CdGeAs_2$ crystals: growth and nonlinear optical properties," in Proc. 17th Nat. Conf. Cryst. Growth Mater., 2015.
9. T. S. Moss, J. C. G. de Sande, and C. Hilsum, "Characterization of $CdGeAs_2$ grown by the float zone technique under microgravity," J. Cryst. Growth, vol. 198–199, pp. 898–903, 1999.
10. American Elements, "Yttrium oxide (Y_2O_3) tablets," Product Specification, 2026.
11. M. Born and E. Wolf, Principles of Optics, 7th ed. Cambridge, UK: Cambridge University Press, 1999.
12. A. Yariv and P. Yeh, Optical Waves in Crystals. New York: Wiley, 1984.
13. G. D. Boyd, E. Buehler, and F. G. Storz, "Linear and nonlinear optical properties of $CdGeAs_2$," Appl. Phys. Lett., vol. 18, no. 8, pp. 301–304,1971.
14. R. L. Aggarwal, D. J. Ripin, J. R. Ochoa, and T. Y. Fan, "Measurement of thermo-optic properties of Y_2O_3 and Lu_2O_3 at 1064 nm," J. Appl. Phys., vol. 98, no. 10, p. 103514, 2005. (Note: the dispersion formula used in this work is adapted from similar temperature-dependent models for Y_2O_3; the specific coefficients correspond to the cited reference.)

